

## Article

# Numerical Investigations on the Effects of Dome Cooling Air Flow on Combustion Characteristics and Emission Behavior in a Can-Type Gas Turbine Combustor

Chenzhen Ji <sup>1</sup> , Wentao Shi <sup>1</sup>, Enlei Ke <sup>1</sup>, Jiaying Cheng <sup>1</sup> , Tong Zhu <sup>1</sup> , Chao Zong <sup>1,2,\*</sup> and Xinyan Li <sup>3</sup> 

<sup>1</sup> School of Mechanical Engineering, Tongji University, Jiading District, Shanghai 201804, China; czji@tongji.edu.cn (C.J.); 2132722@tongji.edu.cn (W.S.); 2030255@tongji.edu.cn (E.K.); ch400t@163.com (J.C.); zhu\_tong@tongji.edu.cn (T.Z.)

<sup>2</sup> Postdoctoral Station of Mechanical Engineering, Tongji University, Shanghai 201804, China

<sup>3</sup> School of Aerospace Engineering, Beijing Institute of Technology, Haidian District, Beijing 100081, China; lixy037@bit.edu.cn

\* Correspondence: zongchao@tongji.edu.cn

**Abstract:** To meet the requirements of achieving higher efficiency and lower NO<sub>x</sub> pollution, the flame temperature in gas turbine combustors increases continually; thus, the effusion-cooling technology has been used to ensure the combustor liner remains within the allowed temperature, by which the combustion characteristics and emission behavior are possibly influenced. In order to investigate the effects of dome cooling air flow on combustion characteristics and NO<sub>x</sub> emissions, three-dimensional combustion simulations for a swirl-stabilized can-type gas turbine combustor are carried out in this work by using the computational fluid dynamics (CFD) method. Through adjusting the ratio of the dome cooling air flow and the dilution cooling air flow, the characteristics of flow field, temperature distribution and NO<sub>x</sub> emissions under each work condition are analyzed. At different ratios of the dome-cooling air flow to the total air flow, the flow velocity field in the region near the center of the combustion chamber is not changed much, while the velocity field near the chamber wall shows a more significant difference. The temperature in the outer recirculation zone within the combustion chamber is effectively reduced as the dome cooling air flow increases. By analyzing the distribution characteristics of the concentration of OH\*, it is demonstrated that the dome cooling air flow does not have a direct effect on the reaction of combustion. It is also found that as the ratio of the dome cooling air flow to the total air flow increases from 0 to 0.15, the value of the NO<sub>x</sub> emissions drops from 28.4 to 26.3 ppmv, about a 7.4% decrease. The distribution of the NO<sub>x</sub> generation rate in the combustion chamber does not vary significantly with the increasing dome cooling air flow. Furthermore, by calculating the residence time in different stages, when the the ratio of the dome cooling air flow to the total air flow varies from 0 to 0.15, the residence time in the pilot stage decreases obviously, from 42 ms to 18 ms. This means that reduction in residence time is the main factor in the decrease of NO<sub>x</sub> emissions when the dome cooling air flow increases.

**Keywords:** gas turbine; effusion cooling; combustor liner; dome cooling; NO<sub>x</sub> emission; Computational Fluid Dynamics; outer recirculation zone



**Citation:** Ji, C.; Shi, W.; Ke, E.; Cheng, J.; Zhu, T.; Zong, C.; Li, X. Numerical Investigations on the Effects of Dome Cooling Air Flow on Combustion Characteristics and Emission Behavior in a Can-Type Gas Turbine Combustor. *Aerospace* **2024**, *11*, 338. <https://doi.org/10.3390/aerospace11050338>

Academic Editors: Ernesto Benini and Andrea Magrini

Received: 29 March 2024

Revised: 16 April 2024

Accepted: 18 April 2024

Published: 25 April 2024



**Copyright:** © 2024 by the authors. Licensee MDPI, Basel, Switzerland. This article is an open access article distributed under the terms and conditions of the Creative Commons Attribution (CC BY) license (<https://creativecommons.org/licenses/by/4.0/>).

## 1. Introduction

The combustor systems of modern high-efficiency, low-emission gas turbine engines have been under continual development and improvement over the last decade [1]. Today's gas turbine combustion systems seek to limit the NO<sub>x</sub> emission value to 25 ppm or less prior to the reduction measures on exhaust gases. Based on the study of the mechanism of NO<sub>x</sub> generation [2,3], stringent regulations governing pollutant emission have led to low-emission combustion technology shifting to lean premixed combustion [4–6]. In lean combustion applications, a larger amount of air is routed into the combustion chamber,

which can apparently reduce the combustion temperatures along with significant reduction in NO<sub>x</sub> emissions.

Lean premixed combustion technology leads to a reduced amount of air available for the combustor liner cooling; thus, it is necessary to develop an optimized combustor liner cooling method. The combustor liner in a modern gas turbine is subjected to very high temperatures and high thermal gradients that severely impact its structural strength. The cooling technology is needed to ensure that the combustor liner remains within the allowed working temperature [7,8]. One of the effective ways to cool a combustor liner is through effusion cooling by perforated walls [9,10]. Effusion cooling [11,12], also known as full-coverage film cooling, has successive rows of cooling holes that interact with each other and form a continuous protective film along the wall. Today, the effusion cooling method is widely and effectively used in gas turbine combustion chambers due to its simple structure, effective cooling performance and relatively low coolant pressure loss.

The cooling effectiveness of effusion cooling is the most focused, and its performance relates to many factors, including the cooling flow angle, modular cooling geometries, flame-cooling flow interaction, swirl flow and so on [13]. Yang et al. [14,15] conducted an experimental and numerical study on the heat-transfer characteristics of tangential effusion cooling for a combustor liner. With a blowing ratio ranging from 2.2 to 17.9, the results of the proposed structure were compared with that of effusion holes based on the flat plate. They found that the overall cooling effectiveness of tangential effusion was about 50% higher than the effusion holes based on the flat plate. Ahmed et al. [16] performed steady-state infrared thermography experiments to calculate the performance of an effusion-cooled combustor liner under reacting and non-reacting conditions. They found that the coolant flame interaction for the reacting experiments impacted the liner cooling effectiveness and led to different overall cooling effectiveness distribution on the liner when compared with the non-reacting experiments. Hermann et al. [17] presented experimental measurements in an effusion-cooled single-sector gas turbine combustor under elevated pressure to investigate flame-cooling-air interaction with modular cooling geometries. They proposed a novel test rig and used particle image velocimetry (PIV), planar laser-induced fluorescence of the hydroxyl radical (OH-PLIF) and coherent anti-Stokes Raman scattering (CARS) to measure the flow field, flame structure and gas-phase temperature, respectively. Isothermal mixing, non-reacting and reacting flow fields as well as flame structure and gas-phase temperature measurements under reacting conditions with parametric variations of swirl intensities and staging have been reported. Based on the measurements of the flow and combustion fields, it was found that the reactive and non-reactive flow fields yielded fundamental differences with respect to the influence of staging. In the non-reacting case, the influence of the mass flow disappeared within the first few millimeters, while in the reacting case, the influences on the flow field and the gas-phase temperature could be observed up to 30 mm inside the flame tube. Wurm et al. [18] conducted experimental studies to deal with the impact of swirl flow on the effusion-cooling performance of an effusion-cooled combustor liner. They found that increasing the overall total pressure drop across the liner led to an improved overall cooling performance and that the 45° heat shield showed increased cooling effectiveness but that the starter film penetration was significantly influenced by the swirl flow.

The use of effusion cooling can reduce the temperature of the combustor wall, but the arrangement of the cooling holes may affect the combustion characteristics and NO<sub>x</sub> emissions at the same time. Zong et al. [19,20] proposed a novel external combustion air adjustment method to redistribute the combustion air of a micro-gas-turbine combustor under the off-design loads. They found that reducing the combustion air ratio controlled the huge increase in CO emission under off-design loads, but also increased the risk of NO<sub>x</sub> emissions, as it led to a significant velocity increase close to the jet shear layers and thus resulted in a longer reaction zone residence time. Zhang et al. [21] numerically investigated the effects of lateral cooling hole configuration on a swirl-stabilized combustor. Two lateral coolant injection designs were proposed, and the results showed that when the incidence

angle was  $15^\circ$ , the NO<sub>x</sub> emissions remained relatively low for all incidence configurations. However, the NO<sub>x</sub> emissions gradually raised as the incidence angle increased. When the lateral incidence was implemented at a larger incidence angle, such as  $30^\circ$ , the cooling effectiveness was maintained above 0.9. In addition, when the coolant incidence direction was opposite to the swirling flow and the incidence angle was set at  $15^\circ$ , it resulted in the highest total pressure loss. Furthermore, Daniel Lörstad et al. [22,23] conducted investigations on the cooling effects of the “soft wall” located on the impingement-cooled combustor wall on the Siemens SGT-800 combustor. By the CFD simulations based on the conjugate heat transfer method, they found that the introduction of a “soft wall” with cooling flow in an existing combustor design led to changes of the cooling layout due to the convection-cooled design, since half of the local cooling flow exited through the “soft wall”. The local cooling at the head of the combustor chamber was significantly improved by the reduced heat load due to the bias flow. It was also mentioned that the “soft wall” also minimized the main flame NO<sub>x</sub> emissions and significantly reduced the levels of thermoacoustic instability. Greifenstein et al. [24,25] also experimentally investigated the mixing processes between main-flow and effusion-cooling air in a swirl-stabilized pressurized single-sector gas turbine combustor by using OH-PLIF and NO-PLIF. They found that a significant case-dependent asymmetry of OH concentration was observed within the primary zone close to the nozzle and the reaction zones were severely impaired by effusion-cooling air. This asymmetry was caused by the lower flame brush, where more intense mixing of effusion-cooling air and fresh gas was observed.

From previous research work, it can be found that the effusion-cooling technology not only reduces the temperature of the combustor liner but also shows some effects on the combustion dynamics and NO<sub>x</sub> emission, which is highly dependent on the design of the combustor liner. Even though there have been some pioneer investigations on the effects of combustor liner cooling on the combustion process and pollution emissions, few systematic and in-depth research works have been reported about this. Therefore, in the current work, the study of effusion-cooled liner effects on a swirl-stabilized can-type gas turbine combustor was conducted by three-dimensional (3D) numerical combustion simulations. Different cooling effects were realized by allocating the ratio of cooling air; in particular, the effects of the dome cooling air flow were focused on in this work. The following sections introduce the geometrical configuration of the gas turbine combustor, numerical model development, model validation, numerical results and discussion to reveal the internal mechanisms affecting NO<sub>x</sub> production by the dome cooling air. Meanwhile, the combustion characteristics and flow behavior in the can-type gas turbine combustor will also be presented and discussed.

## 2. Numerical Modeling

### 2.1. Configuration of Combustor

The dual-axial swirler combustor is fed by natural gas, and its performance test data employed in this study were introduced in our previous work [19,20]. As shown in Figure 1, the dual-axial swirler combustor is composed of the burner, liner and casing parts. The burner has a two-stage fuel supply, of which the outer side is the primary stage with a premixed flame used, and the center is the pilot stage with a diffusion flame adopted. Under practical operating conditions, low-emission concentrations of CO and NO<sub>x</sub> can be obtained simultaneously by different air distribution ratios and flexible fuel supply strategies.

The angled effusion-cooling holes are arranged between the burner and diffusion holes of the liner, with a total row number of 14, and the row spacing of the effusion-cooling holes is 10 mm. Each row is evenly distributed with 60 inclined holes, and each hole is designed in a diameter of 1 mm. Along the axial direction, 4 rows are on the slope of the liner, which are called the dome cooling holes; 10 rows are on the straight wall and called the liner cooling holes. During the operations, the cooling air forms a cooling film inside the liner through the cooling hole to protect the liner from being ablated by the elevated temperature.

Although the fuel used in this study was compressed natural gas (CNG), CNG's main composition and combustion characteristics are similar to that of methane. Therefore, the fuel composition was regarded as pure methane in the subsequent combustion simulation.

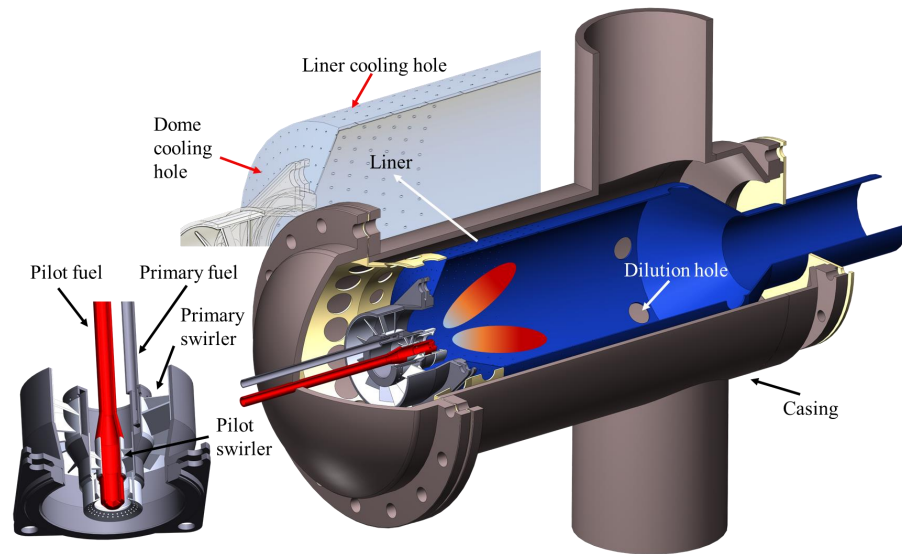


**Figure 1.** Configuration of the dual-axial swirler can-type combustor studied in the current work.

## 2.2. Governing Equations

The three-dimensional, steady-state Reynolds-averaged Navier–Stokes (RANS) equations were used to resolve the flow and combustion regime of the gas turbine can-type combustor within the computational domain:

Continuity equation:

$$\nabla \cdot (\rho \vec{v}) = 0, \quad (1)$$

Momentum equation:

$$\nabla \cdot (\rho \vec{v} \vec{v}) = -\nabla p + \nabla \cdot \bar{\tau}, \quad (2)$$

Energy equation:

$$\nabla \cdot (\rho \vec{v} h) = \nabla \cdot \left( k_{\text{eff}} \nabla T - \sum_j h_j \vec{J}_j \right) + S_R + S_E, \quad (3)$$

Species transportation equation:

$$\nabla \cdot (\rho \vec{v} Y_i) = -\nabla \cdot \vec{J}_i + R_i, \quad (4)$$

where  $\rho$  is the density of the mixture,  $\vec{v}$  is the velocity vector,  $p$  is the pressure,  $\bar{\tau}$  is the stress tensor,  $h$  is the sensible enthalpy,  $k_{\text{eff}}$  is the effective thermal conductivity,  $J$  is the diffusion flux,  $Y$  is the species mass fraction,  $S_R$  is the radiative source term,  $S_E$  is the chemical reaction source term and  $R$  is the net rate of production by chemical reaction. The subscript  $i$  and  $j$  represent species  $i$  and species  $j$ , respectively.

For the closure-of-turbulence equations, the realizable  $k$ - $\epsilon$  turbulence model was used, as it is suitable for simulating complex fluid flow with the swirling flow, flow recirculation and vortex breakdown [14]. For combustion modeling, identification and treatment of the huge difference between turbulence behavior and chemical reaction on a timescale is a challenging problem [26]. A complex reaction zone and slower chemical reactions, such as the formation process of nitrogen oxides, also place high requirements on the prediction accuracy of the elementary reaction process. The eddy dissipation concept (EDC) model was considered for the combustion simulation and prediction of specific species concentration in this work. The EDC model assumes that elementary reactions always occur on a fine scale where the dissipation of turbulence kinetic energy takes place [27]. The

accurate prediction of reaction progress depends on the reasonable evaluation of the spatial scale fraction  $\zeta$  and the mean residence time  $\tau$  of the fine scale by the EDC model [28]:

$$\zeta = C_{\zeta} \left( \frac{\nu \varepsilon}{k^2} \right)^{\frac{1}{4}}, \quad (5)$$

$$\tau = C_{\tau} \left( \frac{\nu}{\varepsilon} \right)^{\frac{1}{2}}, \quad (6)$$

where  $C_{\zeta}$  represents the volume fraction constant and equals 2.1377,  $C_{\tau}$  is a timescale constant and set as 0.4082,  $\nu$  is the kinematic viscosity,  $\varepsilon$  is the turbulent dissipation rate and  $k$  is the turbulent kinetic energy.

The selection of kinetic mechanism is a vital strategy in the numerical simulation of the combustion process. A detailed reaction mechanism, such as GRI-Mech 3.0 [29] or GRI-Mech 2.11 [30,31], is able to exhibit the effects of intermediates on combustion chemistry, but costs extensive computational resources and time as it calculates more elementary reactions. Thus, a reduced kinetic mechanism, which consisted of the 16 components and 35 elementary reactions proposed by Smooke [32], was judged to be suitable for predicting methane/air combustion in the present work. The accuracy of this reaction mechanism has been extensively validated under various conditions including the gas turbine combustion [33,34]. With respect to the prediction of nitrogen oxides, the influence of a high temperature environment on the formation rate of nitrogen oxides was emphatically considered [35,36]. The reduced mechanism in the N/O system introduced by Hanson et al. [37], which consists of 15 elementary reactions, was selected to predict the formation of nitrogen oxides.

The COUPLED algorithm was used for the pressure–velocity coupling, and the pseudo-transient under-relaxation method was employed to improve the computational efficiency and convergence. Most equations, including momentum, energy, turbulence and species transport, were spatially discretized by the second-order upwind scheme. The convergence levels were set to follow the criteria that the residuals for velocity, energy and main species (including CH<sub>4</sub>, O<sub>2</sub>, CO, CO<sub>2</sub> and H<sub>2</sub>O) variables were lower than 10<sup>−6</sup> and the remaining variables were lower than 10<sup>−3</sup>. In Figure 2, the residual of energy represents the convergence of the temperature; the iterative computation of temperature was considered to converge when the residual was less than 10<sup>−6</sup>.

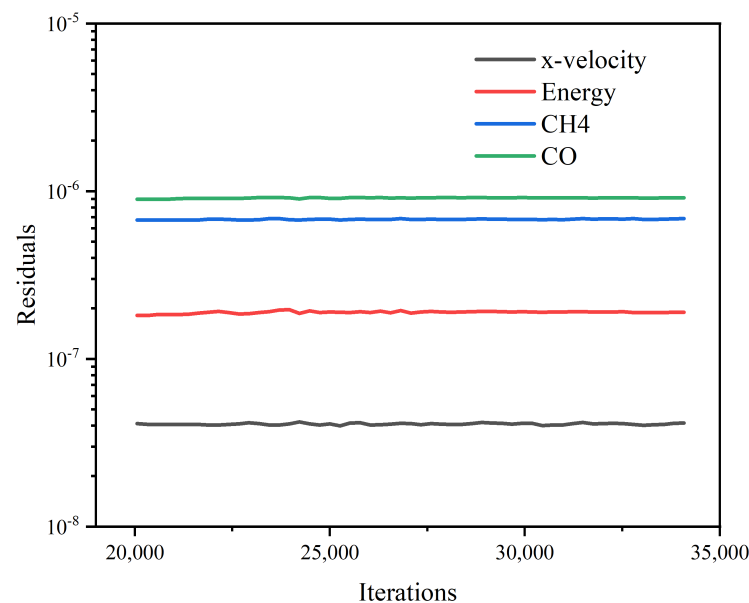


**Figure 2.** The residual plots about the velocity, temperature and concentration fields.

In this work, the core of the combustor chamber (inner channel), including the pre-mixed zone, reaction zone and mixing zone, was selected as the computational domain. The air flow entered into the inner channel through the inlet of the inner and outer swirlers, cooling holes and dilution holes. The flow rate of each path was directly assigned according to the operating-load conditions and air-distribution ratio set at the baseload, as shown in Figure 3a. All the walls of the combustor were assumed to be adiabatic walls in the current simulation.

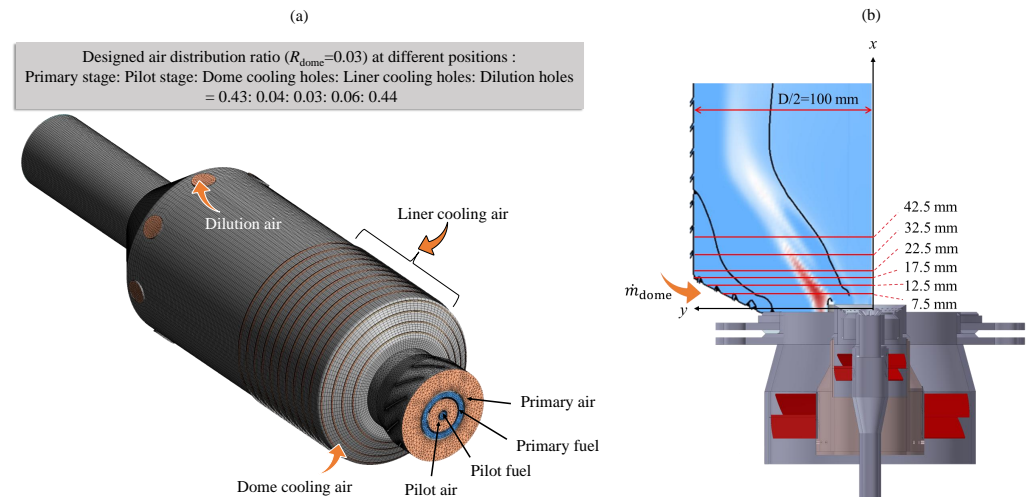


**Figure 3.** (a) Hybrid mesh generation of the dual-axial swirler combustor and air distribution is assigned through several paths: primary stage, pilot stage, dome cooling holes, liner cooling holes and dilution holes. (b) Variables monitoring at the locations of  $x = 7.5, 12.5, 17.5, 22.5, 32.5, 42.5$  mm in the simulations.

### 2.3. Mesh Generation and Independence Study

For the mesh generation of the dual-axial swirler combustor, a hybrid mesh generation method was employed, as shown in Figure 3a. An unstructured grid was generated in the premixed zone, which contained inner and outer swirlers, fuel nozzles and other complex structures, while a structured grid was used in the reaction and mixing zones. The meshes of the two parts were generated independently and then merged at the interfaces. Local mesh quality improvements were carried out to ensure the high numerical accuracy of the modeling.

To accurately predict the combustion process, a mesh independence study was conducted to simulate a nonreactive flow field under a 100% load and a PFP of 9.0%. Three kinds of mesh, with a total number of 3.08, 4.15 and 5.88 million, respectively, were numerically tested. By comparing the velocity profile at the outlet of the swirlers, the mesh with the total number of 4.15 million was selected for the following simulation work as it was able to obtain a good balance between numerical accuracy and computing-time costs.

### 2.4. Setup of the Simulation Cases

The operation parameters refer to the actual operation conditions of a micro gas turbine [19]. Under the baseline condition, the total natural gas flow into the combustion chamber is  $85.8 \text{ Nm}^3/\text{h}$ , of which the volume flow rate of pilot fuel accounts for 15.2%. The total air flow is  $1.16 \text{ kg/s}$ , which enters the internal flow field through the primary swirler, pilot swirler, dome cooling holes, liner cooling holes and dilution holes, respectively. The proportion of each part, as above, is 0.43, 0.04, 0.03, 0.06 and 0.44, respectively. The inlet temperature of the air flow of each of the above is the same, fixed at  $523.5 \text{ K}$ ; meanwhile, the pressure at the outlet of the combustion chamber is set at  $0.393 \text{ MPa}$ .

In the present work, we defined the ratio of the dome cooling air flow to the total air flow as the  $R_{dome}$ , which was 0.03 under the baseline condition. To investigate the influence of dome cooling air on the internal flow field, six cases were investigated, as shown in

Table 1, where the  $R_{dome}$  increased from 0 to 0.15 with an increment of 0.03. It should be noted that the flow rate of the dilution air decreased with the increase in the dome cooling air, while the primary/pilot-stage air and liner cooling air remained constant to ensure the same fuel–air ratio in the reaction zone of the combustion chamber.

Table 1. The setup of simulation cases studied in the current work.

| Proportion of Air Flow through Each Part | Case 1 | Case 2 | Case 3 | Case 4 | Case 5 | Case 6 |
|--|--------|--------|--------|--------|--------|--------|
| primary swirler                          | 0.43   | 0.43   | 0.43   | 0.43   | 0.43   | 0.43   |
| pilot swirler                            | 0.04   | 0.04   | 0.04   | 0.04   | 0.04   | 0.04   |
| dome cooling holes                       | 0      | 0.03   | 0.06   | 0.09   | 0.12   | 0.15   |
| liner cooling holes                      | 0.065  | 0.065  | 0.065  | 0.065  | 0.065  | 0.065  |
| dilution holes                           | 0.465  | 0.435  | 0.405  | 0.375  | 0.345  | 0.315  |

### 3. Results and Discussion

#### 3.1. Validation of the Numerical Model

The numerical model developed in this paper was firstly validated with the swirling methane/air flame 2 (SMA2) case of the Sydney swirl flame database [38,39] as shown in Figure 4. The schematic diagram of the Sydney swirl burner is shown in Figure 4a, and the details of mesh generation are presented in Figure 4b. The axial velocity, temperature, CO and NO distributions were compared between the current simulation, Amani’s numerical results [40] and the experimental measurements as plotted in Figure 4c. It can be observed that the selected combustion reaction mechanism can capture changes of axial speed, temperature and specific species very well by comparison with the experimental data from the SMA2 case. At the same time, it can also predict the actual pollutant emission level of the combustor investigated in this work, as reported in our previous work [20]. Therefore, this confirms that the developed numerical model is suitable for the numerical simulation work on the gas turbine combustion process, which will be discussed in the following sections.

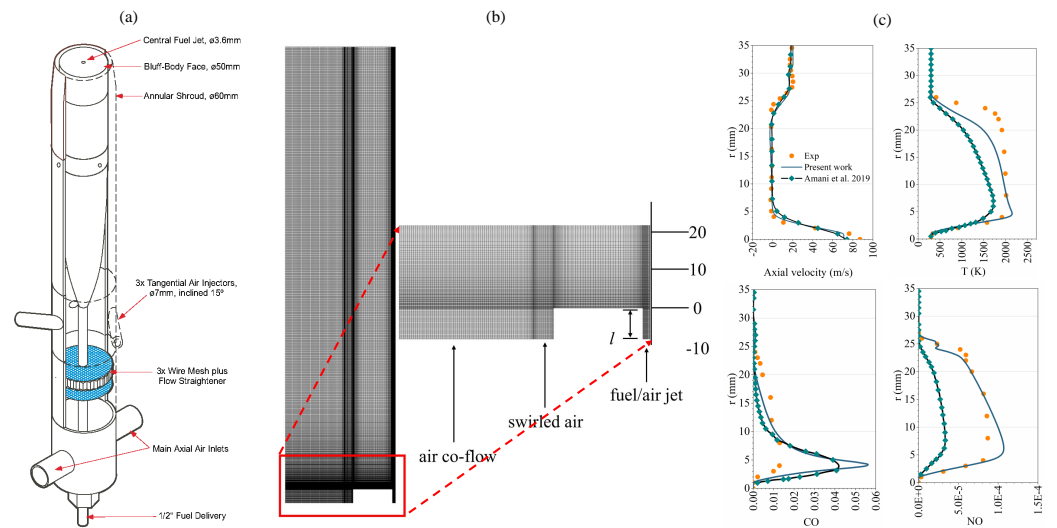
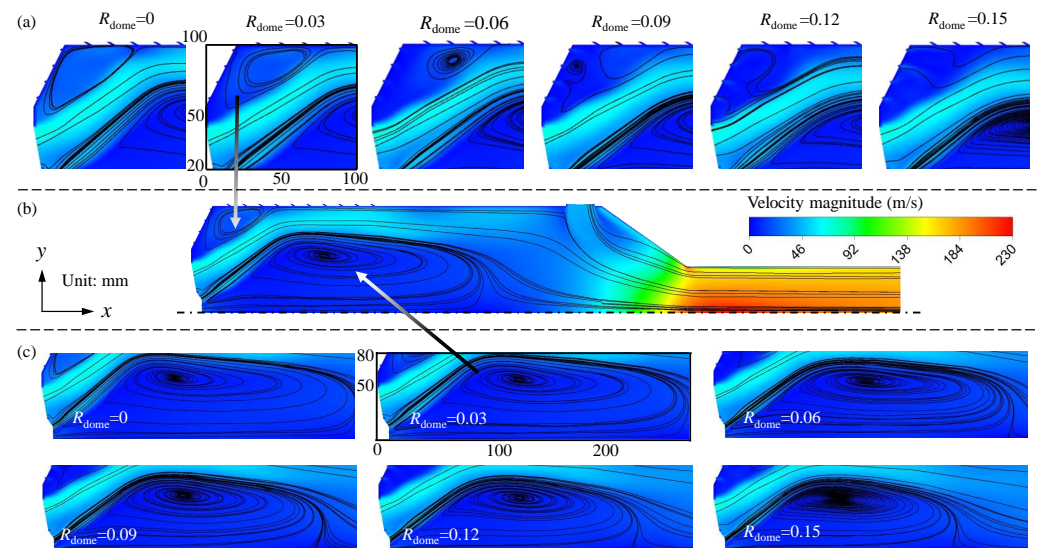


Figure 4. Validations of current numerical model: (a) Experimental setup of SMA2 case of the Sydney swirl flame. (b) Mesh generation for the geometric model of the SMA2 case. (c) Comparison of the numerical and experimental results of the Sydney swirl flame database (green lines with green symbols: simulations by Amani et al. [40]; green lines without any symbols: current numerical work; yellow symbols: the SMA2 experimental data).

### 3.2. Effects of the $R_{\text{dome}}$ on Flow Fields within the Combustor

To investigate the effects of the dome cooling air flow on the combustion process, visualizations of the flow field within the gas turbine can-type combustor are firstly presented under the reaction condition. From Figure 5, it is obvious that with the increase of the  $R_{\text{dome}}$  from 0 to 0.15, the vortex structures in both locations, the outer recirculation zone (ORZ) and the central recirculation zone (CRZ), were significantly changed. As shown in Figure 5a, when the  $R_{\text{dome}}$  was at 0, a vortex in a relative large size close to the corner of the can-type combustor was formed. Actually, in most gas turbine combustor designs, the vortex at the ORZ plays a role in stabilizing the swirling flame. As the flow rate of the dome cooling air increased, the vortex was pushed downward, and its size became smaller when the  $R_{\text{dome}}$  was at 0.03 and 0.06. Once the  $R_{\text{dome}}$  approached 0.09 and even higher, the vortex structure at the ORZ gradually broke up and even almost disappeared when the  $R_{\text{dome}}$  increased to 0.15. The vortex at the CRZ was also apparently affected by the dome cooling air flow. From Figure 5c, it can be seen that when the  $R_{\text{dome}}$  equaled 0, the size of the vortex at the CRZ was biggest, and it became smaller with the increase in the  $R_{\text{dome}}$ .



**Figure 5.** Velocity contours in: (a) The ORZ. (b) The whole combustion chamber. (c) The CRZ under the work conditions when the flow rate ratio of the dome cooling air, the  $R_{\text{dome}}$ , equaled 0, 0.03, 0.06, 0.09, 0.12 and 0.15.

To quantitatively analyze the relationship between dome cooling flow and flame reaction, Figure 6 gives the exact size changes of the CRZ, which were influenced by the increase of the  $R_{\text{dome}}$ . As defined in Figure 6a, the  $D_{\text{CRZ}}$ , the maximum diameter of the CRZ, means the transverse range of velocity shear while the  $L_{\text{CRZ}}$  stands for the axial length from the burner outlet to the critical edge of the CRZ. Figure 6b shows the effects of the  $R_{\text{dome}}$  on the size of the CRZ. It is clearly demonstrated that the diameter of the CRZ, the  $D_{\text{CRZ}}$ , showed a small decrease of about 6 mm when the  $R_{\text{dome}}$  increased from 0 to 0.15. However, the  $R_{\text{dome}}$  exhibited much more influence on the length of the CRZ, the  $L_{\text{CRZ}}$ . The  $L_{\text{CRZ}}$  dropped about 65 mm, which almost reached one quarter of the total length of the CRZ at the  $R_{\text{dome}} = 0$ . Subsequently, a comparison of the calculated velocity profiles under different work conditions was conducted. The velocity profile was selected at different axial locations away from the burner outlet, as marked in Figure 3b, and the velocity profiles at the locations of  $x = 7.5, 12.5, 17.5, 22.5, 32.5, 42.5$  mm are described in Figure 7. The data were extracted from the area close to the inlet of the combustion chamber that contained the ORZ, where the characteristics of velocity changes in the CRZ had not been analyzed at that time. From Figure 7, at a different  $R_{\text{dome}}$ , the flow velocity in the region near the center of the combustion chamber was almost unchanged, while the velocity near the angular vortex region showed a more significant difference. This was consistent with the characteristics of

the vortex structure shown in the streamline diagram. This illustrates the fact that the form of distribution of the effusion-cooling air flow, especially the flow rate ratio of the dome cooling air, the  $R_{dome}$ , shows the impacts on the flow field inside the combustion chamber, which may change the combustion characteristics in a can-type gas turbine combustor.

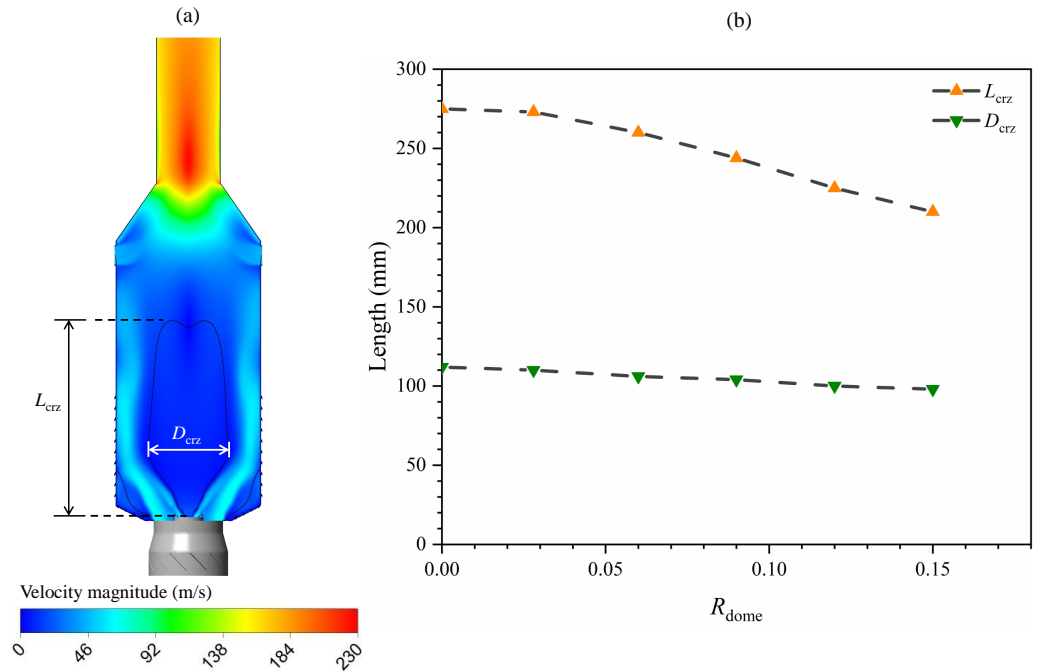


**Figure 6.** (a) Definitions of the length ( $L_{crz}$ ) and width ( $D_{crz}$ ) of the CRZ in a can-type gas turbine combustor. (b) Variation of  $L_{crz}$  and  $D_{crz}$  under the different flow rate ratios of dome cooling air, the  $R_{dome}$ .

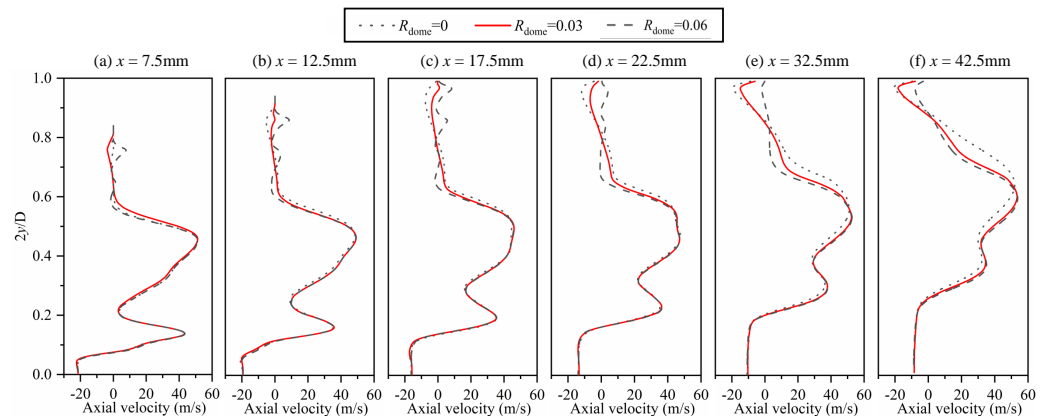


**Figure 7.** Velocity profiles at the locations of  $x = 7.5, 12.5, 17.5, 22.5, 32.5, 42.5$  mm when the flow rate ratio of the dome cooling air, the  $R_{dome}$ , was set at 0, 0.03 and 0.06.

### 3.3. Effects of the $R_{dome}$ on Temperature and Reaction Rate Distributions

Figure 8 illustrates the temperature contours in the combustion chamber under the different flow rates of the dome cooling air flow. The temperature contours with isolines clearly show that the temperature distributions at the ORZ were significantly influenced by the  $R_{dome}$ . The original case without any dome cooling air had an obvious high-temperature zone of about 1200 K (labeled in green) in the ORZ. With the increase of the  $R_{dome}$  from 0 to 0.15, the mean temperature at the ORZ became lower and the size of the high-temperature zone apparently reduced. At the  $R_{dome}$  condition of 0.15, the ORZ was almost filled by low-temperature gas of about 600 K (labeled in blue). However, the

temperature contours at the CRZ were not affected a lot by the increase in the dome cooling air flow.

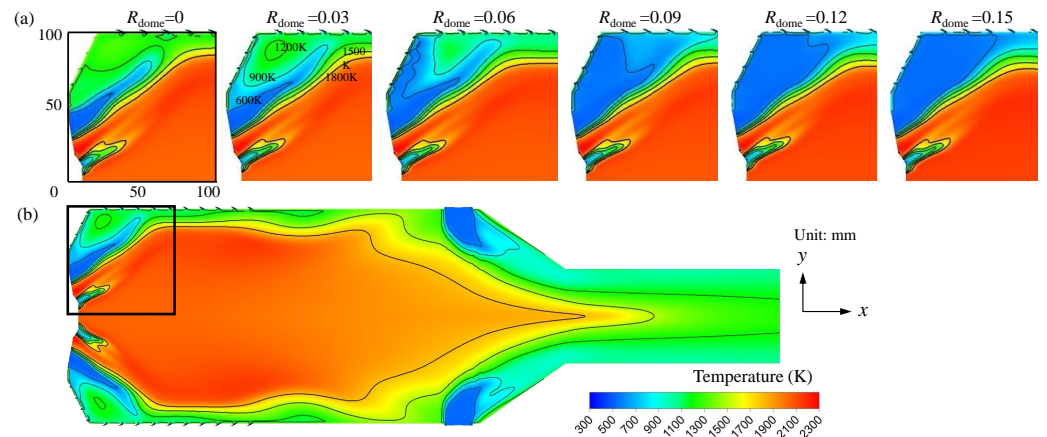


**Figure 8.** Temperature contours in: (a) The ORZ. (b) The whole combustion chamber under the various work conditions when the flow rate ratio of the dome cooling air, the  $R_{dome}$ , varied from 0, 0.03, 0.06, 0.09, 0.12 to 0.15.

Similarly, Figure 9 shows the axial temperature distribution of three simulation cases where the flow rate ratio of the dome cooling air, the  $R_{dome}$ , equaled 0, 0.03 and 0.06. The temperature profile results show similar trends to those of the velocity profile in Figure 7, i.e., there was no obvious variation near the center region, but significant differences occurred at the ORZ. Combined with the results of the temperature contours, it can be found that the temperature in the ORZ within the combustion chamber was effectively reduced as the dome cooling air flow increased. When  $x \geq 32.5$  mm, the temperature over the entire cross section including the ORZ varied little with the  $R_{dome}$ . This illustrates that the dome cooling air flow mainly affected the temperature distribution near the inlet region of the combustion chamber.

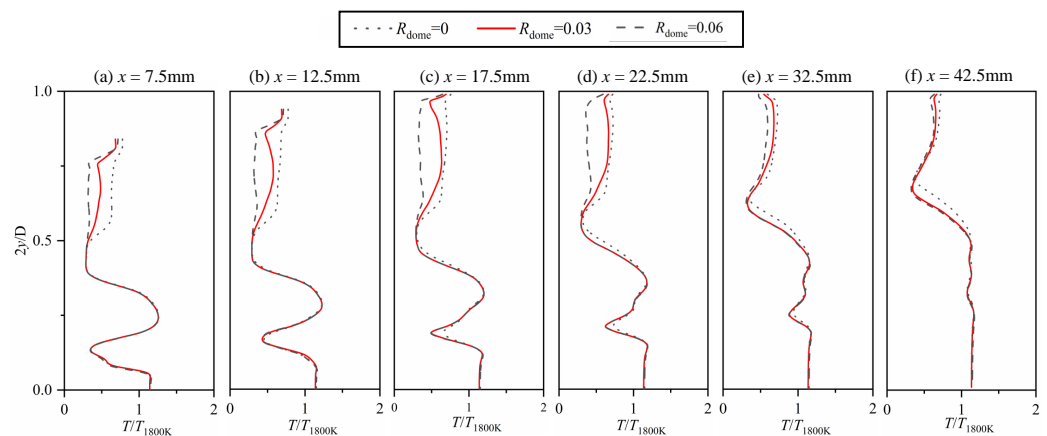


**Figure 9.** Normalized temperature profiles at the locations of  $x = 7.5, 12.5, 17.5, 22.5, 32.5, 42.5$  mm when the flow rate ratio of the dome cooling air, the  $R_{dome}$ , was set at 0, 0.03 and 0.06.

The following will focus on the reaction in the combustor influenced by the  $R_{dome}$ . The magnitude of the heat release rate can be characterized by the concentrations of  $OH^*$ , and in this paper the concentration of  $OH^*$  can also be used to illustrate the morphology of the flames. Figure 10 gives the  $OH^*$  contours in the different  $R_{dome}$  conditions. It was found that there were no significant changes in flame shape by adjusting the ratio of the dome cooling air flow. This demonstrates that the dome cooling air flow does not have a direct impact on the reaction of combustion, but it does change the flow field and temperature distribution in the combustion chamber.

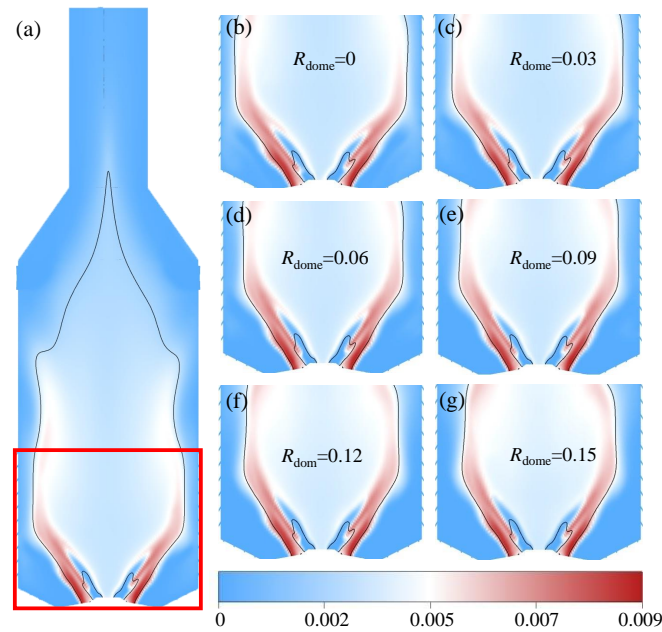


**Figure 10.** OH\* distribution in: (a) The whole combustion chamber. (b–g) The outlet of the burner under the work conditions when the flow rate ratio of the dome cooling air, the  $R_{dome}$ , equaled 0, 0.03, 0.06, 0.09, 0.12 and 0.15.

#### 3.4. Effects of the $R_{dome}$ on the NOx Emission Behavior

The pollutant emission is one of the key parameters for gas turbine combustors. The overall NOx emissions of the combustor at different  $R_{dome}$  were calculated and are shown in Figure 11. The dome cooling air flow had an influence on the reduction of the NOx emissions. When the flow rate ratio of the dome cooling air, the  $R_{dome}$ , was 0, the value of the NOx emission was about 28.4 ppmv. As the  $R_{dome}$  increased to 0.15, the magnitude of the NOx emission decreased to 26.3 ppmv, with a total decrease of 2.1 ppmv, which was about 7.4% of the original emission value. It should be pointed out that all the operating conditions had satisfying NOx emission concentrations that could meet the stringent regulations on NOx emissions as proposed in most countries.

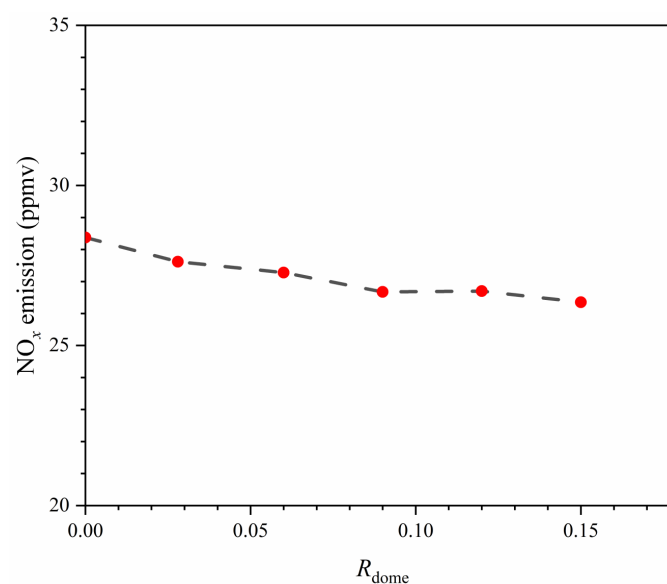


**Figure 11.** NOx emission of the gas turbine combustor when the flow rate ratio of the dome cooling air, the  $R_{dome}$ , varied from 0 to 0.15. (Red dots represent the simulation results of six cases; black dash line is the fitting curve of the simulation results).

In order to further investigate the effect of the dome cooling air flow on NO<sub>x</sub> production, the reaction rates of NO<sub>x</sub> generation at different  $R_{\text{dome}}$  were calculated and plotted in Figure 12. The result obtained was that the  $R_{\text{dome}}$  had almost no effects on the rate of NO<sub>x</sub> production, which was the same trend as presented in Figure 10. The main region of NO<sub>x</sub> generation was concentrated in the zone where the combustion reaction was the most intense, and the combustion reaction did not change when the proportion of dome cooling air increased. Therefore, the distribution of the NO<sub>x</sub> generation rate in the combustion chamber did not vary significantly with the increasing  $R_{\text{dome}}$ .

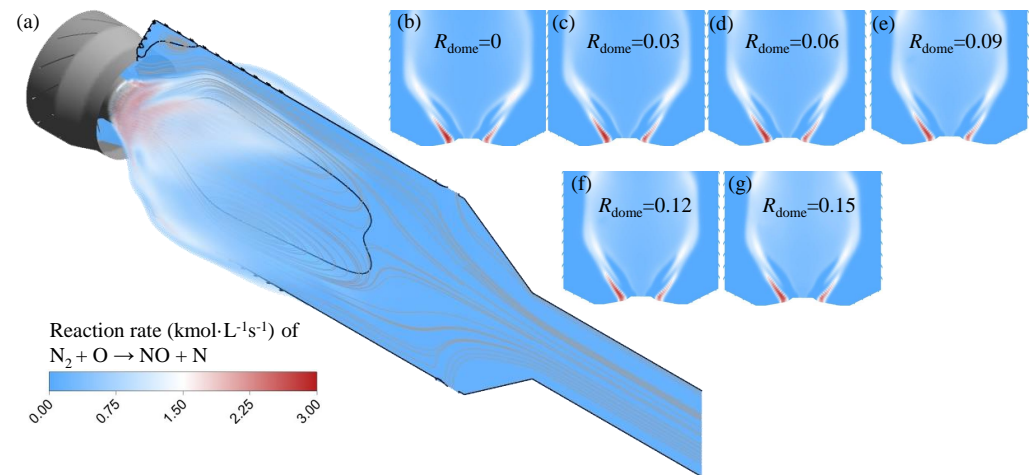


**Figure 12.** Reaction rate of NO<sub>x</sub> contours in (a) The whole combustion chamber. (b–g) The outlet of the burner under the work conditions when the flow rate ratio of the dome cooling air, the  $R_{\text{dome}}$ , was at 0, 0.03, 0.06, 0.09, 0.12 and 0.15.

In addition, Figure 13 shows the axial temperature and reaction rate of the NO<sub>x</sub> generation profiles of three simulation cases where the  $R_{\text{dome}}$  was set at 0, 0.03 and 0.06. The peak of the NO<sub>x</sub> reaction intensity appears where the highest temperature occurs, consistent with previous studies. NO<sub>x</sub> is mainly generated in the CRZ, while it is rarely generated in the ORZ. Although the increase of the dome cooling air flow resulted in a significant decrease in temperature in the ORZ, it had little effect on the total NO<sub>x</sub> production. This suggests that decrease in NO<sub>x</sub> by increasing the  $R_{\text{dome}}$  is not caused by lowering the temperature in the combustion chamber.

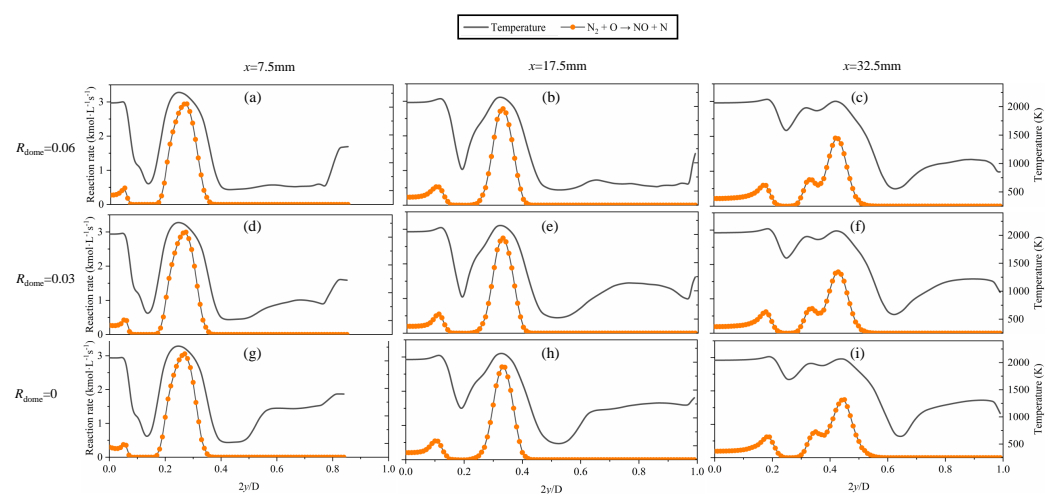


**Figure 13.** Temperature and reaction rate of NO<sub>x</sub> profiles at the locations of  $x = 7.5$  (a,d,g), 17.5 (b,e,h), 32.5 (c,f,i) mm when the flow rate ratio of the dome cooling air, the  $R_{\text{dome}}$ , was set at 0.06, 0.03 and 0.

Residence time is one of the most important factors affecting the generation of NOx. Figure 14 plots the residence time in the pilot stage and primary stage and the mass weighted mean value under different  $R_{\text{dome}}$  conditions. It can be seen from this that as the  $R_{\text{dome}}$  increased from 0 to 0.15, the residence time in the pilot stage decreased significantly, from 42 ms to 18 ms. This means that increasing the proportion of dome cooling air flow can reduce the residence time in the pilot stage, which can lead to a reduction in the generation of NOx in the can-type gas turbine combustor.

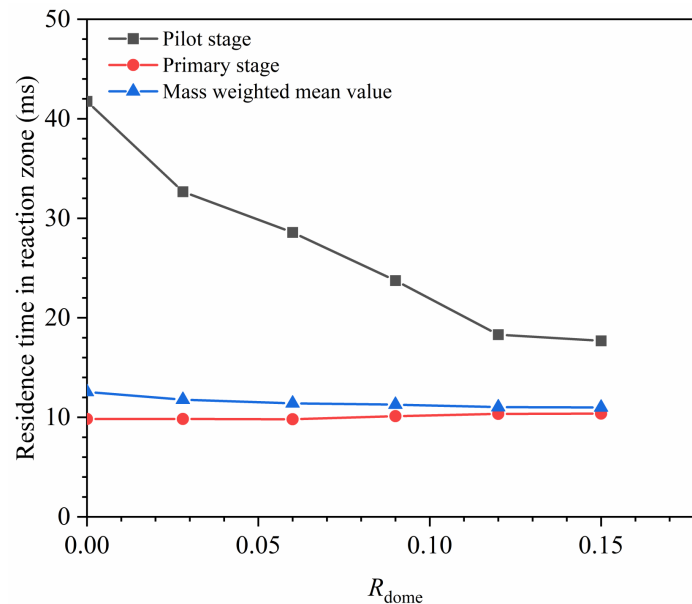


**Figure 14.** Residence time in the reaction zone varies with the flow rate ratio of the dome cooling air, the  $R_{\text{dome}}$ .

#### 4. Conclusions

In order to investigate the effects of dome cooling air flow on combustion characteristics and NOx emissions in a can-type gas turbine combustor, three-dimensional combustion simulations for a swirl-stabilized can-type gas turbine combustor were carried out by using the CFD method. In the simulations, by adjusting the ratio of the dome cooling air flow and the dilution cooling air flow, the gas turbine combustion process under various conditions of dome air flow ratios,  $R_{\text{dome}}$ , were simulated, and the characteristics of flow field, temperature distribution and NOx emission under each condition have been presented and analyzed in detail. Firstly, by validating with the SMA2 case of the Sydney swirl flame database, it was confirmed that the developed numerical model is suitable for numerical simulation work on a gas turbine combustor.

With the increase of the  $R_{\text{dome}}$  from 0 to 0.15, the vortex structures in both regions of the ORZ and the CRZ were significantly changed, especially the vortex in the ORZ, which even broke and disappeared when the  $R_{\text{dome}}$  approached 0.12 and higher. Under different work conditions of the  $R_{\text{dome}}$ , the flow velocity in the region near the center of the combustion chamber was not obviously unchanged, while the velocity near the wall showed a more significant difference. The temperature in the ORZ within the combustion chamber was effectively reduced as the dome cooling air flow increased, while there was little change in temperature distribution in the other regions. Combined with the results of the temperature profiles, when  $x \geq 32.5$  mm, the temperature over the entire cross section including the ORZ varied little with the  $R_{\text{dome}}$ . This illustrates that the dome cooling air flow mainly affects the temperature distribution near the inlet region of the combustion chamber. By analyzing the distribution characteristics of the concentration of OH\*, it was demonstrated that the ratio of the dome cooling air flow did not have a direct impact on the combustion reaction process when the  $R_{\text{dome}}$  increased from 0 to 0.15.

Notably, it was found that the dome cooling air flow could reduce the NO<sub>x</sub> emissions. When the  $R_{\text{dome}}$  was set at 0, the value of the NO<sub>x</sub> emissions was 28.4 ppmv, and as the  $R_{\text{dome}}$  increased to 0.15, the value of the NO<sub>x</sub> emissions decreased to 26.3 ppmv, with a total decrease of 2.1 ppmv, which was equivalent to a 7.4% drop based on the initial value. However, from the analytical results, it was found that the distribution of the NO<sub>x</sub> generation rate in the combustion chamber did not vary a lot with the increasing of the  $R_{\text{dome}}$ . By calculating the residence time in different stages, when the  $R_{\text{dome}}$  varied from 0 to 0.15, the residence time in the pilot stage decreased obviously, from 42 ms to 18 ms. This means that the reduction of residence time is the main factor in the decrease of NO<sub>x</sub> emissions when the dome cooling air flow, the  $R_{\text{dome}}$ , increases.

**Author Contributions:** Conceptualization, C.J., W.S. and C.Z.; methodology, C.J. and W.S.; software, W.S. and J.C.; validation, C.J., W.S. and E.K.; formal analysis, C.J. and W.S.; investigation, C.J., W.S., E.K. and J.C.; resources, C.J. and T.Z.; data curation, C.J., W.S. and C.Z.; writing—original draft preparation, C.J., W.S. and C.Z.; writing—review and editing, C.J., J.C., T.Z., C.Z. and X.L.; visualization, C.J. and X.L.; supervision, C.Z. and X.L.; project administration, T.Z.; funding acquisition, C.J. All authors have read and agreed to the published version of the manuscript.

**Funding:** The authors gratefully acknowledge the financial support of Shanghai Committee of Science and Technology (Grant No. 21ZR1466000).

**Data Availability Statement:** Data are contained within the article.

**Conflicts of Interest:** The authors declare no conflicts of interest.

## Abbreviations

The following abbreviations are used in this manuscript:

|      |                                 |
|------|---------------------------------|
| CFD  | computational fluid dynamics    |
| CNG  | compressed natural gas          |
| CRZ  | central recirculation zone      |
| EDC  | eddy dissipation concept        |
| ORZ  | outer recirculation zone        |
| PIV  | particle image velocimetry      |
| RANS | Reynolds-averaged Navier-Stokes |
| SMA2 | swirling methane/air flame 2    |

## References

- Liu, Y.; Sun, X.; Sethi, V.; Nalianda, D.; Li, Y.G.; Wang, L. Review of modern low emissions combustion technologies for aero gas turbine engines. *Prog. Aerosp. Sci.* **2017**, *94*, 12–45. [[CrossRef](#)]
- Zeldovich, Y.B.; Barenblatt, G.I.; Librovich, V.B.; Makhviladze, G.M. *The Mathematical Theory of Combustion and Explosions*; Consultants Bureau: New York, NY, USA, 1985.
- Siriganano, W.; Merzhabov, A.; De Luca, L. Advances in Combustion Science In Honor of Ya. B. Zelovich. *Prog. Astronaut. Aeronaut.* **1996**, *173*. [[CrossRef](#)]
- Le, X.T.; Nguyen, D.A.; Dinh, C.T. Effect of Two-Head Flared Hole on Film Cooling Performance over a Flat Plate. *Aerospace* **2021**, *8*, 128. [[CrossRef](#)]
- Somarathne, K.; Okafor, E.C.; Hayakawa, A. Emission characteristics of turbulent non-premixed ammonia/air and methane/air swirl flames through a rich-lean combustor under various wall thermal boundary conditions at high pressure. *Combust. Flame* **2019**, *210*, 247–261. [[CrossRef](#)]
- Rivera, J.E.; Gordon, R.L.; Brouzet, D.; Talei, M. Exhaust CO emissions of a laminar premixed propane–air flame interacting with cold gas jets. *Combust. Flame* **2019**, *210*, 374–388. [[CrossRef](#)]
- Huang, Y.; Feng, X.; Lin, Z.; You, Y. Effects of wall cooling with microchannels on swirl combustor performance. *Aerosp. Sci. Technol.* **2020**, *106*, 106160. [[CrossRef](#)]
- Ren, J.; Li, X.; Jiang, H. Conjugate heat transfer characteristics in a highly thermally loaded film cooling configuration with TBC in syngas. *Aerospace* **2019**, *6*, 16. [[CrossRef](#)]
- Tarchi, L.; Facchini, B.; Maiuolo, F.; Coutandin, D. Experimental investigation on the effects of a large recirculating area on the performance of an effusion cooled combustor liner. *J. Eng. Gas Turbines Power* **2012**, *134*, 041505. [[CrossRef](#)]
- Krewinkel, R. A review of gas turbine effusion cooling studies. *Int. J. Heat Mass Transf.* **2013**, *66*, 706–722. [[CrossRef](#)]

11. Shen, Z.; Hu, B.; Li, G.; Zhang, H. Large Eddy Simulation of Pulsed Film Cooling with a Dielectric Barrier Discharge Plasma Actuator. *Aerospace* **2023**, *11*, 28. [CrossRef]
12. Mazzei, L.; Puggelli, S.; Bertini, D. Numerical and Experimental Investigation on an Effusion-Cooled Lean Burn Aeronautical Combustor: Aerothermal Field and Emissions. *J. Eng. Gas Turbines Power* **2019**, *141*, 041006. [CrossRef]
13. Ji, Y.; Ge, B.; Zang, S. Analysis of effusion cooling under realistic swirl reacting flow in gas turbine combustor. *Appl. Therm. Eng.* **2022**, *216*, 119101. [CrossRef]
14. Yang, X.; He, Z.; Qiu, P. Numerical investigations on combustion and emission characteristics of a novel elliptical jet-stabilized model combustor. *Energy* **2019**, *170*, 1082–1097. [CrossRef]
15. Yang, G.; Shao, W.; Zhang, Z. Experimental and numerical study on heat transfer characteristics of tangential effusion cooling for a combustor liner. *Appl. Therm. Eng.* **2022**, *218*, 119374. [CrossRef]
16. Ahmed, S.; Ramakrishnan, K.R.; Ekkad, S.V. Overall cooling effectiveness of effusion cooled can combustor liner under reacting and non-reacting conditions. *J. Therm. Sci. Eng. Appl.* **2022**, *14*, 021009. [CrossRef]
17. Hermann, J.; Greifenstein, M.; Boehm, B.; Dreizler, A. Experimental investigation of global combustion characteristics in an effusion cooled single sector model gas turbine combustor. *Flow Turbul. Combust.* **2019**, *102*, 1025–1052. [CrossRef]
18. Wurm, B.; Schulz, A.; Bauer, H.J.; Gerendas, M. Impact of swirl flow on the cooling performance of an effusion cooled combustor liner. *J. Eng. Gas Turbines Power* **2012**, *134*, 121503. [CrossRef]
19. Zong, C.; Ji, C.; Cheng, J.; Zhu, T. Comparison of adiabatic and conjugate heat transfer models on near-wall region flows and thermal characteristics of angled effusion cooling holes. *Therm. Sci. Eng. Prog.* **2022**, *30*, 101269. [CrossRef]
20. Zong, C.; Ji, C.; Cheng, J. Toward off-design loads: Investigations on combustion and emissions characteristics of a micro gas turbine combustor by external combustion-air adjustments. *Energy* **2022**, *253*, 124194. [CrossRef]
21. Zhang, Y.; Li, J.; Xie, J. Effects of lateral cooling hole configuration on a swirl-stabilized combustor. *Energy* **2022**, *259*, 125002. [CrossRef]
22. Lörstad, D.; Lindholm, A.; Pettersson, J. Siemens SGT-800 industrial gas turbine enhanced to 50MW: Combustor design modifications, validation and operation experience. In *Turbo Expo: Power for Land, Sea, and Air, Proceedings of the ASME Turbo Expo 2013: Turbine Technical Conference and Exposition, San Antonio, TX, USA, 3–7 June 2013*; American Society of Mechanical Engineers: New York, NY, USA, 2013; Volume 55119, V01BT04A038. [CrossRef]
23. Lörstad, D.; Pettersson, J.; Lindholm, A. Emission reduction and cooling improvements due to the introduction of passive acoustic damping in an existing SGT-800 combustor. In *Turbo Expo: Power for Land, Sea, and Air, Proceedings of the ASME Turbo Expo 2009: Power for Land, Sea, and Air, Orlando, FL, USA, 8–12 June 2009*; American Society of Mechanical Engineers: New York, NY, USA, 2009; Volume 48845, pp. 1355–1362. [CrossRef]
24. Greifenstein, M.; Hermann, J.; Boehm, B.; Dreizler, A. Flame-cooling air interaction in an effusion-cooled model gas turbine combustor at elevated pressure. *Exp. Fluids* **2019**, *60*, 1–13. [CrossRef]
25. Greifenstein, M.; Dreizler, A. Investigation of mixing processes of effusion cooling air and main flow in a single sector model gas turbine combustor at elevated pressure. *Int. J. Heat Fluid Flow* **2021**, *88*, 108768. [CrossRef]
26. Wang, Z.; Hu, B.; Fang, A. Analyzing lean blow-off limits of gas turbine combustors based on local and global Damköhler number of reaction zone. *Aerosp. Sci. Technol.* **2021**, *111*, 106532. [CrossRef]
27. Fordoei, E.E.; Mazaheri, K.; Mohammadpour, A. Effects of hydrogen addition to methane on the thermal and ignition delay characteristics of fuel-air, oxygen-enriched and oxy-fuel MILD combustion. *Int. J. Hydrogen Energy* **2021**, *46*, 34002–34017. [CrossRef]
28. ANSYS, Inc. ANSYS Fluent Theory Guide. 2020. Available online: <http://www.ansys.com> (accessed on 17 April 2024).
29. Gregory, P.S.; David, M.G.; Michael, F. GRI-Mech 3.0 Mechanism. 1999. Available online: <http://combustion.berkeley.edu/gri-mech/version30/text30.html> (accessed on 17 April 2024).
30. Kanoshima, R.; Hayakawa, A.; Kudo, T. Effects of initial mixture temperature and pressure on laminar burning velocity and Markstein length of ammonia/air premixed laminar flames. *Fuel* **2022**, *310*, 122149. [CrossRef]
31. Bowman, C.T.; Hanson, R.K.; Davidson, D.F. GRI-Mech 2.11 Mechanism. 1995. Available online: <http://combustion.berkeley.edu/gri-mech/new21/version21/text21.html> (accessed on 17 April 2024).
32. Smooke, M.D. *Reduced Kinetic Mechanisms and Asymptotic Approximations for Methane-Air Flames: A Topical Volume*; Springer: Berlin/Heidelberg, Germany, 1991.
33. Tyliczszak, A.; Boguslawski, A.; Nowak, D. Numerical simulations of combustion process in a gas turbine with a single and multi-point fuel injection system. *Appl. Energy* **2016**, *174*, 153–165. [CrossRef]
34. Zhu, R.; Pan, D.; Ji, C. Combustion instability analysis on a partially premixed swirl combustor by thermoacoustic experiments and modeling. *Energy* **2022**, *211*, 118884. [CrossRef]
35. Correa, S.M. A review of NO<sub>x</sub> formation under gas-turbine combustion conditions. *Combust. Sci. Technol.* **1993**, *87*, 329–362. [CrossRef]
36. Xing, C.; Chen, X.; Qiu, P. Effect of fuel flexibility on combustion performance of a micro-mixing gas turbine combustor at different fuel temperatures. *J. Energy Inst.* **2022**, *102*, 100–117. [CrossRef]
37. Hanson, R.K.; Salimian, S. Survey of rate constants in the N/H/O system. *Combust. Chem.* **1984**, 361–421. [CrossRef]
38. Masri, A.R.; Kalt, P.A.M.; Barlow, R.S. The compositional structure of swirl-stabilized turbulent nonpremixed flames. *Combust. Flame* **2004**, *137*, 1–37. [CrossRef]

- 
39. Al-Abdeli, Y.M.; Masri, A.R. Stability characteristics and flowfields of turbulent non-premixed swirling flames. *Combust. Theory Model.* **2003**, *7*, 731–766. [[CrossRef](#)]
  40. Amani, E.; Rahdan, P.; Pourvosoughi, S. Multi-objective optimizations of air partitioning in a gas turbine combustor. *Appl. Therm. Eng.* **2019**, *148*, 1292–1302. [[CrossRef](#)]

**Disclaimer/Publisher’s Note:** The statements, opinions and data contained in all publications are solely those of the individual author(s) and contributor(s) and not of MDPI and/or the editor(s). MDPI and/or the editor(s) disclaim responsibility for any injury to people or property resulting from any ideas, methods, instructions or products referred to in the content.